HHS Public Access

Author manuscript

Cell Chem Biol. Author manuscript; available in PMC 2017 October 20.

Published in final edited form as:

Cell Chem Biol. 2016 October 20; 23(10): 1282–1293. doi:10.1016/j.chembiol.2016.09.001.

Endoplasmic Reticulum Proteostasis Influences the Oligomeric State of an Amyloidogenic Protein Secreted from Mammalian Cells

John J. Chen[1,5], **Joseph C. Genereux**[1,2,5,6], **Eul Hyun Suh**[2], **Vincent F. Vartabedian**[1], **Bibiana Rius**[1], **Song Qu**[1], **Maria T.A. Dendle**[2], **Jeffery W. Kelly**[1,2,3], and **R. Luke Wiseman**[1,4,7,*]

[1]Department of Molecular & Experimental Medicine, The Scripps Research Institute, 10550 North, Torrey Pines Road, MEM 220, La Jolla, CA 92037, USA

[2]Department of Chemistry, The Scripps Research Institute, La Jolla, CA 92037, USA

[3]The Skaggs Institute for Chemical Biology, The Scripps Research Institute, La Jolla, CA 92037, USA

[4]Department of Chemical Physiology, The Scripps Research Institute, La Jolla, CA 92037, USA

SUMMARY

Transthyretin (TTR) is a tetrameric serum protein associated with multiple systemic amyloid diseases. In these disorders, TTR aggregates in extracellular environments through a mechanism involving rate-limiting dissociation of the tetramer to monomers, which then misfold and aggregate into soluble oligomers and amyloid fibrils that induce toxicity in distal tissues. Using an assay established herein, we show that highly destabilized, aggregation-prone TTR variants are secreted as both native tetramers and non-native conformations that accumulate as high-molecular-weight oligomers. Pharmacologic chaperones that promote endoplasmic reticulum (ER) proteostasis of destabilized TTR variants increase their fraction secreted as a tetramer and reduce extracellular aggregate populations. In contrast, disrupting ER proteostasis reduces the fraction of destabilized TTR secreted as a tetramer and increases extracellular aggregates. These results identify ER proteostasis as a factor that can affect conformational integrity and thus toxic aggregation of secreted amyloidogenic proteins associated with the pathology of protein aggregation diseases.

[*]Correspondence: wiseman@scripps.edu.
[5]Co-first author
[6]Present address: Department of Chemistry, University of California, Riverside, Riverside, CA 92521, USA
[7]Lead Contact

AUTHOR CONTRIBUTIONS

J.J.C., J.C.G., .E.H.S., J.W.K., and R.L.W. designed the research. J.J.C., J.C.G., E.H.S., V.F.V., B.R., S.Q., M.T.A.D., and R.L.W. designed and performed the experiments. J.J.C., J.C.G., V.F.V., B.R., S.Q., M.T.A.D., and R.L.W. interpreted and analyzed the data. J.J.C., J.C.G., E.H.S., and R.L.W. wrote the manuscript.

SUPPLEMENTAL INFORMATION

Supplemental Information includes Supplemental Experimental Procedures and five figures and can be found with this article online at http://dx.doi.org/10.1016/j.chembiol.2016.09.001.

INTRODUCTION

The extracellular aggregation of destabilized, misfolding-prone proteins is linked to degenerative phenotypes in over 30 protein aggregation diseases commonly referred to as amyloid diseases (Eisele et al., 2015). These maladies include Alzheimer's disease, Creutzfeldt-Jakob disease, and systemic amyloid diseases. In these disorders, secreted amyloidogenic proteins aggregate into oligomers and amyloid fibrils that are toxic to postmitotic tissues. Genetic and pharmacologic evidence suggests a causal relationship between extracellular toxic aggregation of amyloidogenic proteins and tissue degeneration, demonstrating that protein aggregation is a predominant driving force in amyloid disease pathogenesis (Eisele et al., 2015). Many risk factors have been identified that predispose individuals to toxic aggregation of amyloidogenic proteins including destabilizing mutations, aging, and the composition and activity of extracellular chaperoning pathways (Wyatt et al., 2013). However, the biologic factors that influence the onset and progression of toxic protein aggregation in amyloid disease pathogenesis remain poorly defined.

One biologic factor that can influence the toxic aggregation of amyloidogenic proteins is the activity of endoplasmic reticulum (ER) pathways involved in folding, trafficking, and degradation of the secretory proteome, collectively referred to as ER proteostasis pathways (Chen et al., 2015; Powers et al., 2009). These pathways can facilitate secretion of destabilized, albeit folded, amyloidogenic proteins from mammalian cells, leading to increased concentrations of amyloidogenic proteins in extracellular environments such as serum. This promotes concentration-dependent aggregation of amyloidogenic proteins into toxic oligomers and amyloid fibrils. Remodeling ER proteostasis reduces the secretion and extracellular aggregation of destabilized, aggregation-prone variants of amyloidogenic proteins such as transthyretin (TTR) and immunoglobulin light chain (Chen et al., 2014; Cooley et al., 2014; Plate et al., 2016; Shoulders et al., 2013). This highlights the importance of ER proteostasis in dictating the extracellular concentration of amyloidogenic protein available for proteotoxic aggregation. The importance of ER proteostasis in amyloid disease pathology is also evident from the correlation between secretion, serum levels, and disease severity in patients expressing destabilizing, amyloidogenic variants of TTR (Sekijima et al., 2005).

ER proteostasis could also influence extracellular protein aggregation by altering the quality of amyloidogenic proteins secreted to the extracellular space. Protein misfolding is an obligate step in amyloid formation (Knowles et al., 2014). Disruption of ER proteostasis (i.e., ER stress) increases the population of misfolded proteins within the ER and overwhelms ER proteostasis pathways (Chen et al., 2015; Powers et al., 2009). This challenges the ability of destabilized, amyloidogenic proteins to attain a natively folded conformation. Thus, ER stress could profoundly influence the conformational integrity, and thus the aggregation propensity, of amyloidogenic proteins secreted to the extracellular space. Consistent with this prediction, ER stress promotes the trafficking of misfolded glycosylphosphatidylinositol-anchored proteins such as the prion protein to the cell surface where they are then directed to the lysosome for degradation (Satpute-Krishnan et al., 2014). Furthermore, ER stress increases secretion of the HSP40 co-chaperone ERdj3 in complex with destabilized, amyloidogenic proteins in a mechanism proposed to protect the

extracellular environment from misfolded aggregation-prone protein conformations that can be secreted during ER stress (Genereux et al., 2015). However, the impact of ER stress, or broadly ER proteostasis, on the conformation and stability of a secreted, amyloidogenic protein has not been demonstrated.

One challenge in investigating a role for ER proteostasis in the conformational integrity of secreted amyloidogenic proteins is the difficulty of determining protein conformation in complex biologic environments such as the extracellular space, where secreted protein concentrations are generally low. We address this challenge by developing an assay to monitor the oligomeric state of amyloidogenic TTR variants secreted from mammalian cells. TTR is a serum protein that functions as a native tetramer to transport thyroxine and retinol binding protein (Eisele et al., 2015). However, TTR tetramer dissociation and subsequent aggregation into soluble oligomers and amyloid fibrils is implicated in the onset and pathology of diverse diseases including familial amyloid polyneuropathy and familial amyloid cardiomyopathy (Eisele et al., 2015). Here, we establish an assay that utilizes a non-cell-permeable kinetic stabilizer of the TTR tetramer in combination with a fluorogenic assay to quantify secreted TTR tetramers in conditioned media prepared on mammalian cells. Using this approach, we show that highly destabilized, aggregation-prone TTR variants can be secreted in non-tetrameric conformations that accumulate as high-molecular-weight soluble aggregates. Pharmacologic chaperones increase secretion of destabilized TTR variants as tetramers and reduce extracellular populations of TTR aggregates by stabilizing TTR tetramers in the ER. In contrast, ER stress reduces the fraction of TTR secreted as the native tetramer and increases extracellular populations of soluble TTR aggregates. These results show that ER proteostasis influences the oligomeric state of amyloidogenic TTR secreted from mammalian cells. This indicates that imbalances in ER proteostasis can directly promote extracellular protein aggregation associated with amyloid disease pathology by influencing the conformational integrity of secreted amyloidogenic proteins.

RESULTS

Small-Molecule Fluorogenic TTR Kinetic Stabilizers Can Be Employed to Measure TTR Tetramers Secreted from Mammalian Cells

Small-molecule fluorogenic TTR ligands such as compound **1** (Figure 1A) fluoresce after they covalently react with one or both of the two thyroxine binding sites within the native TTR tetramer (Choi et al., 2010). Two key advantages of these probes are that they only bind to the native TTR tetramer, and they remain “dark” until formation of the covalent adduct within the TTR thyroxine binding pocket. This allows for selective monitoring of native TTR tetramer levels independent of monomers and/or soluble oligomers. Compound **1** has been used to quantify TTR tetramer levels in human serum where TTR concentrations range from 3 to 8 μM (Rappley et al., 2014). We evaluated whether this molecule could also be employed to quantify TTR tetramers in media conditioned on mammalian cells where TTR concentrations are significantly lower than those observed in serum (100–300 nM). We chose HEK293 cells for these experiments because these cells do not synthesize endogenous TTR, show similar secretion efficiencies measured for transfected ^{FT}TTRs compared with

liver-derived HepG2 cells, and have been previously used to define how alterations in ER proteostasis influence secretion of destabilized, amyloidogenic proteins including TTR (Chen et al., 2014; Plate et al., 2016; Shoulders et al., 2013).

We added compound **1** (10 μM) to conditioned media collected from HEK293 cells overexpressing wild-type TTR (TTR^{WT}) or mock-transfected cells. This media was separated by anion-exchange chromatography using a UPLC System, and TTR-compound **1** conjugate fluorescence was monitored as described previously (Rappley et al., 2014). The addition of compound **1** to media containing TTR^{WT} revealed a set of peaks showing compound **1**-TTR conjugate fluorescence that was not present in mock-transfected controls (Figure 1B). The retention time of these peaks is comparable with that of recombinant TTR^{WT} added to cell media, indicating that these peaks are due to the TTR tetramer (Figure S1A).

Our ability to quantify the low levels of TTR^{WT} tetramer conjugate fluorescence in conditioned media with this UPLC assay is compromised by a large background signal observed near the elution time of the tetramer (Figure 1B). This background band has been observed previously and results from the high concentrations of bovine serum proteins (e.g., albumin) present in cell culture media (Rappley et al., 2014). To address this issue, we incorporated a tandem FLAG tag sequence between the ER signal sequence and the N terminus of mature TTR ($^{FT}TTR^{WT}$; Figure 1C). The negatively charged FLAG tags increase the retention time of TTR tetramers on anion-exchange columns, without influencing the stability of the native tetramer (Rappley et al., 2014; Schneider et al., 2001). We observed a new set of compound **1**-TTR conjugate fluorescent peaks at a later elution time in media conditioned for 16 hr on cells expressing $^{FT}TTR^{WT}$ (Figure 1D). This later elution time corresponds with that observed for recombinant $^{FT}TTR^{WT}$ (Figure S1B) and allows for more effective quantification of TTR tetramers in conditioned media. We then confirmed that the addition of 10 μM of compound **1** to conditioned media containing $^{FT}TTR^{WT}$ saturated the **1**-TTR conjugate fluorescence signal (Figure S1C). Furthermore, we used immunopurification (IP)/mass spectrometry (MS) to show that the majority of secreted $^{FT}TTR^{WT}$ is cysteinylated and/or sulfated (Figure S1D). These modified subunits integrate into the homo- and hetero-tetramers that comprise the 8 tetramer peaks observed by our UPLC assay. These modifications are in agreement with what has been seen before for TTR and other FLAG-tagged proteins (Kingsbury et al., 2008; Schmidt et al., 2012; Zhang and Kelly, 2003). While these modifications could have modest effects on TTR stability (Kingsbury et al., 2008; Schneider et al., 2001; Zhang and Kelly, 2003), these modifications are not predicted to globally impact the stability of secreted TTR tetramers.

These results show that the TTR-compound **1** conjugate fluorescence UPLC assay is a useful strategy for quantifying secreted ^{FT}TTR tetramers in conditioned media prepared on mammalian cells. Although this approach is currently limited to cells that do not express endogenous TTR (owing to the large background signal observed in our UPLC assay), this model system provides an opportunity to define how alterations in ER proteostasis influence secretion of TTR and resolve fundamental cell biology questions related to the relationship between ER proteostasis and extracellular protein misfolding and aggregation.

Destabilized, Amyloidogenic TTR Tetramers Are Unstable in Conditioned Media

To examine the effects of disease-associated TTR mutations on secreted TTR tetramer levels, we focused on four TTR variants: TTR^{A25T}, TTR^{L55P}, TTR^{V30M}, and TTR^{V122I}. These variants were selected based on the decreased kinetic and/or thermodynamic stability of the TTR tetramer, reflected by the $t_{1/2}$ of tetramer dissociation, as a measure of kinetic stability, and the C_m of urea denaturation, as a measure of thermodynamic stability (Sekijima et al., 2005). We employed the above-mentioned compound **1**-TTR conjugate fluorescence UPLC assay to measure TTR tetramer levels in media conditioned for 16 hr on HEK293 cells expressing $^{FT}TTR^{A25T}$, $^{FT}TTR^{L55P}$, $^{FT}TTR^{V30M}$, or $^{FT}TTR^{V122I}$ (Figure 2A). We observed similar tetramer levels for the stable $^{FT}TTR^{WT}$ and the $^{FT}TTR^{V122I}$ and $^{FT}TTR^{V30M}$ variants. Gel-filtration chromatography shows that secreted $^{FT}TTR^{WT}$ in conditioned media migrates at a molecular weight consistent with the native tetramer and identical to that observed for recombinant $^{FT}TTR^{WT}$ (Figure S2A and Chen et al., 2014). This suggests that these ^{FT}TTR variants primarily exist as native tetramers in conditioned media. However, highly destabilized $^{FT}TTR^{A25T}$ and $^{FT}TTR^{L55P}$ displayed lower tetramer levels than the more stable variants (Figure 2B), despite being present in similar total concentrations (Figure S2B). To further demonstrate this point, we normalized the conjugate fluorescence derived from **1** (a measure of TTR tetramers) to the relative amounts of total TTR (measured by SDS-PAGE/immunoblotting) for each ^{FT}TTR variant. This showed that the fraction of total secreted TTR existing as a tetramer for $^{FT}TTR^{A25T}$ and $^{FT}TTR^{L55P}$ was reduced by >80% and 50% relative to $^{FT}TTR^{WT}$, respectively (Figure 2C). Importantly, we also showed that the highly destabilized $^{FT}TTR^{A25T}$ is stable in conditioned media for >40 hr, indicating that reductions in tetramer levels cannot be explained by aberrant proteolysis during the incubation with compound **1** (Figure S2C). Taken together, the above results indicate that significant populations of $^{FT}TTR^{A25T}$ and $^{FT}TTR^{L55P}$ in conditioned media are in non-tetrameric conformations.

Dissociation of the native TTR tetramer is the rate-limiting step for TTR aggregation into toxic soluble oligomers and amyloid fibrils (Eisele et al., 2015). Thus, the high non-tetrameric population of destabilized TTR variants in conditioned media could assemble into aggregates. We measured soluble TTR aggregates in media conditioned for 16 hr on HEK293 cells expressing $^{FT}TTR^{A25T}$, $^{FT}TTR^{L55P}$, $^{FT}TTR^{V30M}$, or $^{FT}TTR^{V122I}$ using clear native (CN)-PAGE/immunoblotting (Chen et al., 2014). This showed high levels of TTR aggregates in conditioned media containing $^{FT}TTR^{A25T}$ (Figure 2D). These high levels of aggregates are consistent with low levels of $^{FT}TTR^{A25T}$ tetramers observed by our UPLC assay (Figure 2C). Interestingly, gel-filtration chromatography demonstrated that nearly all $^{FT}TTR^{A25T}$ in conditioned media migrates as high-molecular-weight soluble oligomers, with no significant amount of $^{FT}TTR^{A25T}$ identified in the fractions containing the native tetramer (Chen et al., 2014) (Figure S2A). Combined with our UPLC results (Figures 2B and 2C), this indicates that the majority (>80%) of the $^{FT}TTR^{A25T}$ in conditioned media exists as soluble aggregates. Similarly, we observe a significant amount of soluble TTR aggregates in media conditioned on cells expressing $^{FT}TTR^{L55P}$ (Figure 2D). This is consistent with the 50% lower levels of $^{FT}TTR^{L55P}$ tetramers observed compared with $^{FT}TTR^{WT}$ (Figure 2C). In contrast, no significant accumulation of TTR-soluble oligomers was observed in media conditioned on cells expressing $^{FT}TTR^{V30M}$, $^{FT}TTR^{V122I}$,

or $^{FT}TTR^{WT}$ (Figure 2D). These results suggest that highly destabilized TTR variants are either secreted as tetramers that rapidly dissociate in media during the conditioning or in non-tetrameric conformations that can accumulate as aggregates in conditioned media.

Pharmacologic Chaperoning of Destabilized TTR Variants in the ER Increases Tetramers and Reduces Aggregates in Conditioned Media

Cell-permeable TTR kinetic stabilizers, such as tafamidis (Taf), bind and stabilize TTR tetramers to prevent dissociation and subsequent aggregation (Razavi et al., 2003). These molecules also increase secretion of highly destabilized TTR variants, such as TTR^{A25T} (Chen et al., 2014; Sekijima et al., 2005). This increased secretion is proposed to result from a pharmacologic chaperoning mechanism wherein intracellular binding of Taf to one or both of the two thyroxine binding sites of the TTR tetramer stabilizes the tetrameric structure in the ER and promotes trafficking through the secretory pathway (Sekijima et al., 2005). We examined this mechanism by monitoring the populations of total TTR, TTR aggregates, and TTR tetramers in media conditioned on HEK293 cells expressing $^{FT}TTR^{WT}$, $^{FT}TTR^{L55P}$, or $^{FT}TTR^{A25T}$ in the presence or absence of Taf.

The presence of Taf did not increase total TTR levels of $^{FT}TTR^{WT}$ or $^{FT}TTR^{L55P}$ in conditioned media (Figures 3A and 3B). This is consistent with previous results showing that cell-permeable kinetic stabilizers do not increase secretion of $^{FT}TTR^{WT}$ (Sekijima et al., 2005). However, we observe a 2-fold increase in total $^{FT}TTR^{A25T}$ in conditioned media, reflecting pharmacologic chaperoning of this highly destabilized TTR variant (Chen et al., 2014; Sekijima et al., 2005). As expected, because of the report by Chen et al. (2014), Taf also reduced aggregate populations of $^{FT}TTR^{L55P}$ and $^{FT}TTR^{A25T}$ in conditioned media (Figure 3A). This suggests that the binding of TTR tetramers by Taf in the ER stabilize tetramers throughout the secretion process, as well as in conditioned media, preventing aggregation into soluble oligomers.

We next quantified TTR tetramers in conditioned media samples containing secreted ^{FT}TTR variants using our compound **1** conjugate fluorescence UPLC assay. Although Taf and compound **1** bind the same thyroxine binding sites on the TTR tetramer, the covalent nature of compound **1** binding allows this fluorogenic ligand to efficiently displace Taf within the tetramer, allowing accurate quantification of secreted TTR tetramers by compound **1**-TTR conjugate fluorescence. This effect has been demonstrated previously in human serum (Rappley et al., 2014). Consistent with this, Taf did not influence **1**-$^{FT}TTR^{WT}$ conjugate fluorescence in conditioned media (Figures 3C and 3D), demonstrating the efficacy of compound **1** displacement of Taf in our system and showing that the presence of Taf does not influence our ability to accurately measure secreted TTR tetramers using the covalent TTR kinetic stabilizer compound **1**.

Interestingly, the addition of Taf during conditioning increased $^{FT}TTR^{L55P}$ and $^{FT}TTR^{A25T}$ tetramers in media (Figures 3D–3F). Taf increased $^{FT}TTR^{L55P}$ tetramers 2-fold relative to vehicle (Figures 3D and 3E). This increase is consistent with the Taf-dependent reduction in $^{FT}TTR^{L55P}$-soluble oligomers (Figure 3A). The addition of Taf during the conditioning also increased the media concentration of $^{FT}TTR^{A25T}$ tetramers (Figures 3D and 3F). This is consistent with the significant reduction in $^{FT}TTR^{A25T}$ soluble oligomers afforded by Taf

treatment (Figure 3A). These results show that cell-permeable, small-molecule TTR kinetic stabilizers such as Taf can bind and stabilize TTR tetramers in the ER, as well as in the extracellular space, to increase the population of destabilized TTR secreted in the native tetrameric conformation and reduce extracellular populations of soluble aggregates.

Tafamidis-Sulfonate Is a Non-Cell-Permeable TTR Kinetic Stabilizer that Selectively Binds Secreted TTR Tetramers

The next question we wanted to investigate is the exact nature of the oligomeric state of TTR secreted from mammalian cells. Taf stabilizes TTR tetramers in the ER and maintains this stabilized tetramer throughout the secretion process and in the extracellular space. However, the ER stabilization of TTR tetramers afforded by Taf prevents us from defining the oligomeric state of TTR secreted from mammalian cells. For this type of analysis, we require a TTR kinetic stabilizer that selectively and rapidly stabilizes TTR tetramers only upon secretion to the extracellular environment. The crystal structure of Taf bound to the two thyroxine binding sites of TTR tetramer shows that the carboxylate group at the 6-position of the benzoxazole ring resides at the periphery of the thyroxine binding site near the outside of the TTR tetramer (Bulawa et al., 2012). This suggests that we could replace the carboxylate functionality of Taf with a sulfonate moiety at this position without disrupting the capacity to bind and stabilize TTR tetramers. The addition of a sulfonate at this position, which has a lower pKa than a carboxylate, should limit the cell permeability of Taf, preventing intracellular stabilization of TTR tetramers in the ER and allowing selective stabilization of TTR tetramers, but only once secreted to the media. Toward-ward that aim, we synthesized Taf-SO_3^- and confirmed its identity and purity (Figures 4A, S3A, and S3B).

Inhibition of pH-induced TTR aggregation is an established assay to measure the capacity for small molecules like Taf to bind and stabilize TTR tetramers (Razavi et al., 2003; Sekijima et al., 2005). The addition of increasing equivalents of Taf-SO_3^- to recombinant TTR^{WT} shows a dose-dependent reduction in pH-induced aggregation, with complete inhibition observed at 1.5 equivalents of Taf-SO_3^- relative to the TTR tetramer (Figure 4B). This inhibition of aggregation is nearly identical to that observed with Taf (Bulawa et al., 2012), confirming that Taf-SO_3^- efficiently binds and stabilizes TTR tetramers.

Cell-permeable TTR kinetic stabilizers such as Taf, compound **1**, thyroxine (T4), and flufenamic acid increase the secretion of highly destabilized TTR variants such as TTR^{A25T} from mammalian cells through pharmacologic chaperoning of TTR tetramers in the ER (Figures 3A and 3B and Chen et al., 2014; Sekijima et al., 2005). This is shown by the increased levels of $^{FT}TTR^{A25T}$ in media conditioned on HEK293 cells treated with these different cell-permeable kinetic stabilizers (Figure 4C). However, the addition of Taf-SO_3^- did not increase $^{FT}TTR^{A25T}$ levels in conditioned media. This shows that Taf-SO_3^- is unable to pharmacologically chaperone this destabilized TTR variant in the ER. Collectively, these results indicate that Taf-SO_3^- retains its ability to bind and stabilize extracellular TTR tetramers, but is not able to act as a pharmacologic chaperone within the ER. Thus, Taf-SO_3^- can be employed to selectively stabilize TTR tetramers only upon secretion to conditioned media and evaluate the relative populations of TTR secreted from mammalian cells as tetramers and non-tetrameric conformations.

Highly Destabilized TTR Variants Can Be Secreted in Non-Native Conformations

In order to define the conformation of TTR secreted from mammalian cells, we initially measured total, aggregate, and tetramer levels of TTR in media conditioned for 16 hr on HEK293 cells expressing $^{FT}TTR^{L55P}$ in the presence of vehicle, Taf, or Taf-SO_3^-. The addition of Taf-SO_3^- reduced aggregate levels of $^{FT}TTR^{L55P}$ >75%, mirroring the reduction in aggregates observed in Taf-treated cells (Figures 5A and 5B). However, neither Taf nor Taf-SO_3^- significantly influenced total $^{FT}TTR^{L55P}$ levels in conditioned media (Figures 5A and 5B). These results indicate that Taf-SO_3^- kinetically stabilizes $^{FT}TTR^{L55P}$ tetramers in the extracellular space, preventing TTR aggregation into soluble oligomers. Consistent with this prediction, the addition of Taf-SO_3^- increased $^{FT}TTR^{L55P}$ tetramer levels in conditioned media 2-fold relative to vehicle-treated controls, as measured by our UPLC assay (Figures 5C and S4A). This increase is nearly identical to that observed in Taf-treated cells. These results indicate that $^{FT}TTR^{L55P}$ is predominantly secreted as the native tetramer, which can be stabilized by Taf-SO_3^- in the extracellular space. In addition, these results show that $^{FT}TTR^{L55P}$ aggregates observed in media conditioned in the absence of Taf or Taf-SO_3^- primarily result from the dissociation of secreted $^{FT}TTR^{L55P}$ tetramers and subsequent aggregation during the media conditioning and incubation with **1**.

We also performed an identical analysis using media conditioned for 16 hr on HEK293 cells expressing $^{FT}TTR^{A25T}$. The addition of Taf-SO_3^- did not significantly increase total $^{FT}TTR^{A25T}$ levels in conditioned media, further highlighting the inability of this molecule to pharmacologically chaperone destabilized TTR tetramers in the ER (Figures 5A and 5D). However, unlike Taf, the addition of Taf-SO_3^- reduced extracellular $^{FT}TTR^{A25T}$ soluble aggregates by only 50% when compared with untreated controls (Figures 5A and 5D). This suggests that a population of $^{FT}TTR^{A25T}$ is secreted from mammalian cells in a non-tetrameric conformation that is refractory to stabilization by Taf-SO_3^-.

To examine this further, we measured $^{FT}TTR^{A25T}$ tetramer levels in conditioned media and observed that addition of Taf-SO_3^- increased $^{FT}TTR^{A25T}$ tetramer levels as compared with vehicle-treated cells (Figures 5E and S4B). Importantly, we observe no change in the $^{FT}TTR^{A25T}$ tetramer levels in conditioned media that was prepared in the presence of Taf-SO_3^- and then incubated for 0–12 hr prior to addition of compound **1**, demonstrating that Taf-SO_3^- stabilizes these tetramers in the extracellular space (Figure S4C). In order to compare the relative $^{FT}TTR^{A25T}$ tetramer levels in conditioned media prepared in the presence of Taf (where we observe >90% reduction in aggregates) or Taf-SO_3^- (where we observe a 50% reduction in aggregates), we normalized the observed $^{FT}TTR^{A25T}$ tetramer levels to the amounts of total $^{FT}TTR^{A25T}$ determined by SDS-PAGE. This normalization is necessary to account for the 2-fold increase in total $^{FT}TTR^{A25T}$ afforded by Taf-dependent pharmacologic chaperoning of TTR tetramers in the ER (Figures 5A and 5D). This approach shows that Taf-SO_3^- stabilizes only 65% of the $^{FT}TTR^{A25T}$ tetramer population in the native tetramer, as compared with Taf (Figure 5F). This supports the notion that this highly destabilized TTR variant is secreted from cells as both a tetramer that can be stabilized by Taf-SO_3^- and in a non-tetrameric conformation (e.g., aggregate or misfolded monomer) that is insensitive to Taf-SO_3^--dependent stabilization.

Thapsigargin-Induced ER Stress Reduces the Fraction of $^{FT}TTR^{A25T}$ Secreted as a Tetramer

Imbalances in ER proteostasis (i.e., ER stress) could influence the conformation of $^{FT}TTR^{A25T}$ secreted as a native tetramer. ER stress induced by thapsigargin (Tg) reduces the fraction of total $^{FT}TTR^{A25T}$ secreted from mammalian cell culture models (Shoulders et al., 2013). However, the impact of Tg-induced ER stress on the oligomeric state of secreted $^{FT}TTR^{A25T}$ has not been determined. We utilized SDS-PAGE, CN-PAGE, and UPLC assays to define the impact of Tg-induced ER stress on the oligomeric state of this destabilized TTR variant in conditioned media.

We conditioned media containing Taf-SO_3^- for 16 hr on HEK293 cells expressing $^{FT}TTR^{A25T}$ in the presence or absence of Tg. We confirmed Tg-induced ER stress in these cells by showing increased expression of the ER-stress-responsive chaperone BiP in cell lysates (Figure S5A). As reported previously (Shoulders et al., 2013), Tg reduces total $^{FT}TTR^{A25T}$ levels in conditioned media by 25% (Figures 6A and 6B). Despite this decrease in total $^{FT}TTR^{A25T}$, we observed an increase in TTR aggregates in media conditioned in the presence of Tg (Figures 6A and 6B). To better define the impact of Tg on extracellular $^{FT}TTR^{A25T}$ aggregates, we normalized the observed populations of soluble aggregates to the total amount of TTR measured by SDS-PAGE. This normalization takes into account the reduced total $^{FT}TTR^{A25T}$ in conditioned media prepared in the presence of Tg (Figure 6B). This analysis indicates that Tg increases the normalized TTR aggregate levels 2-fold (Figure 6C).

Next, we used our compound **1**-TTR conjugate fluorescence UPLC assay to show that Tg treatment reduces secreted $^{FT}TTR^{A25T}$ tetramer levels in conditioned media by 60% (Figures 6D and S5B). Normalizing these tetramer signals to account for the Tg-dependent reduction in total $^{FT}TTR^{A25T}$ demonstrates that Tg reduces normalized tetramer levels by 50% (Figure 6E). Lower doses of Tg similarly reduce the relative fraction of $^{FT}TTR^{A25T}$ secreted as the native tetramer (Figures S5C–S5E). This Tg-dependent reduction in tetramer secretion is consistent with the Tg-dependent 2-fold increase in $^{FT}TTR^{A25T}$ aggregate levels (Figure 6C). This suggests that treatment with Tg shifts a population of $^{FT}TTR^{A25T}$ that is normally secreted as the native tetramer to a population that accumulates as extracellular soluble aggregates. Interestingly, reducing expression of $^{FT}TTR^{A25T}$ in HEK293 cells attenuates, but does not ablate, the Tg-dependent reduction in tetramer secretion (Figure S5F). This suggests that this effect is sensitive to ER proteostasis load, indicating that tissues with high secretory load are likely to be most susceptible to ER-stress-dependent alterations in the quality of secreted TTR. Interestingly, Tg similarly reduces the amount of $^{FT}TTR^{WT}$ secreted as the native tetramer by 15% (Figures 6F, 6G, and S5G).

The addition of Tg alters the distribution of peaks observed for $^{FT}TTR^{A25T}$ (Figure S5B) and $^{FT}TTR^{WT}$ (Figure 6F) in our UPLC assay. IP/MS analysis reveals that this results from a modest reduction in secretion of posttranslationally modified $^{FT}TTR^{WT}$ accompanied by a corresponding increase in the population of unmodified protein (Figure S5H). However, these modest alterations in TTR posttranslational modifications induced by Tg do not appear sufficient to explain the 2-fold decrease in $^{FT}TTR^{A25T}$ tetramer secretion we observed.

DISCUSSION

Here, we address the question of how ER proteostasis influences the oligomeric state of secreted TTR, an amyloidogenic protein involved in multiple amyloid diseases. We establish an assay to quantify TTR tetramers secreted from mammalian cells. This assay takes advantage of two small molecules: (1) the non-cell-permeable small-molecule TTR kinetic stabilizer Taf-SO_3^- that stabilizes TTR tetramers upon secretion to the extracellular space and (2) the fluorogenic TTR small-molecule kinetic stabilizer compound **1** that fluoresces upon binding and covalent attachment to TTR tetramers. Using these molecules, we show that highly destabilized TTR variants such as TTR^{A25T} can be secreted as both the native tetramer and in non-native conformations that accumulate as soluble aggregates in the extracellular environment. Pharmacologic chaperoning of these destabilized TTRs in the ER increases their secretion as native tetramers and reduces the accumulation of extracellular soluble oligomers. In contrast, disrupting ER proteostasis reduces the population of TTR secreted as the native tetramer and increases extracellular concentrations of soluble aggregates. These results show that alterations in ER proteostasis can directly influence the conformational integrity, and thus aggregation propensity, of secreted TTR in the extracellular space. The experimental approach described herein provides a new opportunity to further examine the mechanism of TTR aggregation and identify new biologic factors that influence the conformational integrity and aggregation propensity of secreted TTR.

A major implication of our findings is that disruptions of ER proteostasis in tissues secreting amyloidogenic proteins such as TTR could influence their disease-associated extracellular aggregation at distal sites. In this model, imbalances in hepatic ER proteostasis could reduce the conformational integrity of secreted TTR, facilitating extracellular formation of toxic aggregates. These types of imbalances could be induced by hepatic ER stress or organismal aging, both of which can disrupt ER proteostasis in the liver (Brown and Naidoo, 2012). Clinical evidence supports the potential involvement of this type of mechanism in TTR amyloid disease. For example, domino liver transplant recipients receiving livers expressing destabilized TTRs develop TTR amyloid deposition at a considerably faster rate as compared to the donor. (Llado et al., 2010; Stangou et al., 2005). Similarly, transcriptional profiling of livers from mice overexpressing TTR^{WT} suggests that the expression of stress-responsive regulatory factors inversely correlate with the distal deposition of TTR amyloid fibrils on the heart (Buxbaum et al., 2012). These results indicate that alterations in liver ER proteostasis promote the extracellular aggregation and distal deposition of toxic TTR oligomers on the heart. Our results show that imbalances in ER proteostasis can increase secretion of TTR in non-native conformations that accumulate as soluble aggregates, revealing a potential mechanism to explain the relationship between ER proteostasis and toxic aggregation of secreted TTRs that could contribute to the distal deposition of TTR oligomers in human disease.

Disruptions in ER proteostasis could also promote the secretion and subsequent extracellular aggregation of other misfolded proteins. ER stress is implicated in the onset and pathology of many protein aggregation diseases including Alzheimer's disease, Creutzfeldt-Jakob disease, and retinitis pigmentosa (Hetz and Mollereau, 2014; Hiramatsu et al., 2015; Roussel et al., 2013). While it is difficult to discern cause-and-effect relationships for ER stress in the

pathogenesis of these disorders, our results suggest that alterations in ER proteostasis (e.g., ER stress) could promote extracellular aggregation through the secretion of aggregation-prone proteins in non-native conformations. Consistent with this prediction, ER stress increases the trafficking of misfolded PrP proteins to the cell surface (Satpute-Krishnan et al., 2014). Furthermore, misfolded conformations of amyloidogenic proteins such as the amyloid precursor protein can be secreted to extracellular environments in complex with the ER-stress-induced co-chaperone ERdj3 (Genereux et al., 2015). However, the impact of ER stress on the extracellular aggregation of these misfolded proteins remains to be defined. Our work establishes a new experimental strategy that can be adapted to other amyloidogenic or aggregation-prone proteins to evaluate how ER stress influences their proteotoxic aggregation in downstream secretory environments such as the extracellular space.

Interestingly, the increased secretion of TTR variants in non-tetrameric conformations may reflect a mechanism to promote restoration of ER proteostasis during ER stress. While ER proteostasis pathways are traditionally thought to prevent the trafficking of misfolded or non-native conformations, the secretion of misfolded protein conformations could provide a mechanism to relieve the burden of misfolded ER proteins that accumulate during ER stress. Consistent with this mechanism, misfolded prion proteins trafficked to the cell surface in response to ER stress are directed to the lysosome for degradation through a mechanism called rapid ER-stress-induced export (Satpute-Krishnan et al., 2014). Similarly, ER stress increases secretion of the HSP40 co-chaperone ERdj3 to the extracellular space, which is predicted to protect the extracellular environment from misfolded and/or aggregation-prone proteins secreted during ER stress (Genereux et al., 2015). ERdj3 can also be secreted in complex with destabilized, aggregation-prone proteins including TTR^{A25T}, providing a mechanism to preemptively protect the extracellular environment from misfolded protein conformations (Genereux et al., 2015). While these pathways are likely effective at preventing toxic misfolding and/or aggregation of non-native proteins secreted during ER stress, dysregulation of these pathways induced by genetic or aging-related factors could compromise extracellular proteostasis maintenance, potentially explaining the age-dependence of many protein aggregation diseases.

Surprisingly, our results show that pharmacologic chaperoning of destabilized TTR tetramers in the ER offers an advantage for reducing extracellular aggregates of highly destabilized TTR variants. While Taf-dependent stabilization of $^{FT}TTR^{A25T}$ tetramers in the ER nearly ablates extracellular aggregate load, selective stabilization of secreted $^{FT}TTR^{A25T}$ using Taf-SO_3 only partially reduces extracellular aggregates. This importance of intracellular pharmacologic chaperoning to ameliorate extracellular protein aggregation has implications in the establishment of new small-molecule approaches to treat TTR and other amyloid diseases. Our results suggest that non-cell-permeable molecules will be less effective in their ability to attenuate disease toxicity, as they will not prevent secretion of non-native conformations that can accumulate extracellularly as toxic aggregates. In contrast, cell-permeable molecules such as Taf would be favorable as these types of pharmacologic chaperones have the most potential to stabilize the entire population of protein in extracellular environments.

In addition, targeting ER proteostasis pathways could provide a unique opportunity to broadly attenuate the toxic extracellular protein aggregation associated with diverse protein aggregation diseases. One such strategy is to activate unfolded protein response (UPR)-associated transcription factors that endogenously regulate ER protein folding, trafficking, and degradation pathways (Chen et al., 2015). Activation of these transcription factors has previously been shown to reduce the secretion and subsequent aggregation of amyloidogenic variants of TTR and immunoglobulin light chain (Chen et al., 2014; Cooley et al., 2014; Plate et al., 2016; Shoulders et al., 2013). Adapting ER proteostasis through activation of UPR-associated transcription factors could also influence the conformational integrity of amyloidogenic proteins secreted to extracellular environments. Thus, our results reveal another mechanism by which targeting ER proteostasis through UPR-associated transcription factor activation or other approaches could impact extracellular proteotoxic aggregation.

SIGNIFICANCE

Many human amyloid diseases are causatively associated with the extracellular aggregation of proteins that deposit as amyloid fibrils on postmitotic tissues. Risk factors associated with this pathologic protein aggregation include destabilizing mutations in amyloidogenic proteins, aging, and the composition and activity of extracellular chaperoning pathways. However, the biologic pathways that influence the extracellular aggregation of amyloidogenic proteins are largely undefined. Here, we establish a new assay to define the oligomeric state of the amyloidogenic protein transthyretin (TTR) secreted from mammalian cells. In vitro TTR aggregation proceeds through a mechanism involving dissociation of the native tetramer to monomers that then misfold and aggregate into the soluble oligomers and amyloid fibrils implicated in TTR amyloid disease pathogenesis. Interestingly, we show that highly destabilized, aggregation-prone TTR variants can be secreted from mammalian cells in non-native conformations that promote their extracellular aggregation. Intracellular stabilization of TTR using cell-permeable small-molecule kinetic stabilizers, which bind to the native tetramer, increase secretion of destabilized TTRs as tetramers and attenuate extracellular aggregation through a pharmacologic chaperoning mechanism. However, disrupting the protein-folding pathways within the endoplasmic reticulum (ER) responsible for the folding and trafficking of TTR can increase secretion of destabilized TTR tetramers in non-native conformations and increase extracellular aggregate loads. These results show that intracellular alterations in ER pathways involved in the folding and trafficking can influence the quality, and thus aggregation propensity, of amyloidogenic proteins such as TTR secreted to extracellular environments. This reveals ER protein-folding pathways as a new biologic factor the altered activity of which can contribute to the pathologic aggregation of amyloidogenic proteins involved in human disease and suggests that targeting these pathways provides a new opportunity to attenuate the toxic aggregation associated with amyloid disease pathology.

EXPERIMENTAL PROCEDURES

Immunoblotting, CN-PAGE, and SDS-PAGE

CN-PAGE was performed on conditioned media prepared on HEK293 cells expressing ^{FT}TTR variants using a 4%–16% gradient native PAGE gel (Life Technologies) as described previously (Chen et al., 2014). SDS-PAGE was performed on conditioned media or whole-cell lysates using 15% Tris-glycine gels. CN-PAGE and SDS-PAGE gels were transferred onto a nitrocellulose membrane (Bio-Rad) for immunoblotting. Membranes were blocked and then incubated with primary antibodies. Primary antibodies were then detected using appropriate IRDye-conjugated secondary antibodies and then analyzed using the Odyssey Infrared Imaging System (Li-COR Biosciences).

Measurement of TTR Tetramers in Conditioned Media

HEK293 cells overexpressing ^{FT}TTR variants were plated on poly-D-lysine-coated plates. Fresh media was added to the cells and incubated in the presence of vehicle, Taf, or Taf-SO_3^-, as indicated. Conditioned media was diluted 1:1 into water containing **1** to reach the indicated final concentration. This media was stored at ambient temperature prior to UPLC analysis to allow for modification of TTR tetramers. Media samples were separated over a HiQ anion-exchange column in 25 mM Tris (pH 7.0) and 1 mM EDTA with a linear gradient of 1 M NaCl using the ACQUITY UPLC H-Class Bio System (Waters). Fluorescence of TTR conjugates was observed by excitation at 328 nM and monitoring emission at 430 nM. Peaks were integrated using Empower 3 software according to the manufacturer instructions.

Synthesis of Taf-SO_3^-

Taf-SO_3^- was synthesized in an analogous manner to Taf (Razavi et al., 2003).

2-(3,5-Dichlorophenyl)benzo[d]oxazole (**2a**). 2-Hydroxyaniline (3 g, 29 mmol) and 3.5-dichorobenzoyl chloride (5.8 g, 29 mmol) were dissolved in pyridine (0.082 mmol) and tetrahydrofuran (THF) and stirred overnight, the pyridine salt was filtered, and the reaction mixture concentrated in vacuo. The crude mixture was dissolved in ethyl acetate, washed with HCl (1*N*) and brine, and the ethyl acetate evaporated to yield a crude solid (4.450 g) which was washed with hexanes and used without further purification. This crude solid (2 g) was dissolved in xylene, and *p*-toluenesulfonic acid (6.77 g, 35.6 mmol) was added and the mixture refluxed. The crude product was crystallized from DMSO and ethyl ether and washed with hexanes to yield the needle-shaped crystal product (net yield 89.8%).

2-(3,5-Dichlorophenyl)benzo[d]oxazole-6-chlorosulfonicacid(**2b**). **2a** (400mg, 1.5 mmol) was dissolved in chloroform and added dropwise to ice-cold neat $HClSO_3$. The reaction mixture was heated at 125°C for 1 hr under argon, quenched with ice water, extracted with ethyl acetate, and washed with sodium bicarbonate, water, and brine, followed by drying to pure product (403 mg, 1.1 mmol, 74%).

2-(3,5-Dichlorophenyl)benzo[d]oxazole-6-sulfonic acid (Taf-SO_3^-). **2b** (200 mg, 0.57 mmol) was dissolved in 1:1 THF/water in the presence of 4 equiv of LiOH and stirred overnight. After completion by thin-layer chromatography, the reaction mixture was washed

with ethyl acetate to extract the residual starting material, and the aqueous layer acidified to pH 3 with HCl. The product was then extracted with THF and washed with brine to yield a light-brownish-yellow solid, which was recrystallized from ethyl acetate to yield the white solid product Taf-SO_3^- (24 mg, 0.36 mmol, 64%). We confirmed the identity and purity of Taf-SO_3^- using both liquid chromatography (LC)-MS (Figure S3A) and ^1H nuclear magnetic resonance (NMR) (Figure S3B). Note that the identity of the two possible meta positions substitutions is ambiguous by LC-MS and NMR; however, previous a previous report found that modifications at these positions led to similar binding and stabilization of TTR (Razavi et al., 2003).

Statistical Methods

Unless otherwise indicated, all p values were calculated using a paired or unpaired (noted) Student's t test.

Supplementary Material

Refer to Web version on PubMed Central for supplementary material.

ACKNOWLEDGMENTS

We thank Ryan Paxman, Lars Plate, Angelo Solania, Dennis Wolan, and Evan Powers (TSRI) for experimental help and critical reading of this manuscript. We thank the NIH (DK102635 and NS092829) and the Amyloidosis Foundation (R.L.W.) for financial support. J.C.G. was supported by the NIH (HL099245) and an American Heart Association Postdoctoral Fellowship.

REFERENCES

Brown MK, Naidoo N. The endoplasmic reticulum stress response in aging and age-related diseases. Front. Physiol. 2012; 3:263. [PubMed: 22934019]

Bulawa CE, Connelly S, Devit M, Wang L, Weigel C, Fleming JA, Packman J, Powers ET, Wiseman RL, Foss TR, et al. Tafamidis, a potent and selective transthyretin kinetic stabilizer that inhibits the amyloid cascade. Proc. Natl. Acad. Sci. USA. 2012; 109:9629–9634. [PubMed: 22645360]

Buxbaum JN, Tagoe C, Gallo G, Walker JR, Kurian S, Salomon DR. Why are some amyloidoses systemic? Does hepatic “chaperoning at a distance” prevent cardiac deposition in a transgenic model of human senile systemic (transthyretin) amyloidosis? FASEB J. 2012; 26:2283–2293. [PubMed: 22362898]

Chen JJ, Genereux JC, Qu S, Hulleman JD, Shoulders MD, Wiseman RL. ATF6 activation reduces the secretion and extracellular aggregation of destabilized variants of an amyloidogenic protein. Chem. Biol. 2014; 21:1564–1574. [PubMed: 25444553]

Chen JJ, Genereux JC, Wiseman RL. Endoplasmic reticulum quality control and systemic amyloid disease: impacting protein stability from the inside out. IUBMB Life. 2015; 67:404–413. [PubMed: 26018985]

Choi S, Ong DS, Kelly JW. A stilbene that binds selectively to transthyretin in cells and remains dark until it undergoes a chemoselective reaction to create a bright blue fluorescent conjugate. J. Am. Chem. Soc. 2010; 132:16043–16051. [PubMed: 20964336]

Cooley CB, Ryno LM, Plate L, Morgan GJ, Hulleman JD, Kelly JW, Wiseman RL. Unfolded protein response activation reduces secretion and extracellular aggregation of amyloidogenic immunoglobulin light chain. Proc. Natl. Acad. Sci. USA. 2014; 111:13046–13051. [PubMed: 25157167]

Eisele YS, Monteiro C, Fearns C, Encalada SE, Wiseman RL, Powers ET, Kelly JW. Targeting protein aggregation for the treatment of degenerative diseases. Nat. Rev. Drug Discov. 2015; 14:759–780. [PubMed: 26338154]

Genereux JC, Qu S, Zhou M, Ryno LM, Wang S, Shoulders MD, Kaufman RJ, Lasmezas CI, Kelly JW, Wiseman RL. Unfolded protein response-induced ERdj3 secretion links ER stress to extracellular proteostasis. EMBO J. 2015; 34:4–19. [PubMed: 25361606]

Hetz C, Mollereau B. Disturbance of endoplasmic reticulum proteostasis in neurodegenerative diseases. Nat. Rev. Neurosci. 2014; 15:233–249. [PubMed: 24619348]

Hiramatsu N, Chiang WC, Kurt TD, Sigurdson CJ, Lin JH. Multiple mechanisms of unfolded protein response-induced cell death. Am. J. Pathol. 2015; 185:1800–1808. [PubMed: 25956028]

Kingsbury JS, Laue TM, Klimtchuk ES, Theberge R, Costello CE, Connors LH. The modulation of transthyretin tetramer stability by cysteine 10 adducts and the drug diflunisal. Direct analysis by fluorescence-detected analytical ultracentrifugation. J. Biol. Chem. 2008; 283:11887–11896. [PubMed: 18326041]

Knowles TP, Vendruscolo M, Dobson CM. The amyloid state and its association with protein misfolding diseases. Nat. Rev. Mol. Cell Biol. 2014; 15:384–396. [PubMed: 24854788]

Llado L, Baliellas C, Casasnovas C, Ferrer I, Fabregat J, Ramos E, Castellote J, Torras J, Xiol X, Rafecas A. Risk of transmission of systemic transthyretin amyloidosis after domino liver transplantation. Liver Transpl. 2010; 16:1386–1392. [PubMed: 21117248]

Plate L, Cooley CB, Chen JJ, Paxman RJ, Gallagher CM, Madoux F, Genereux JC, Dobbs W, Garza D, Spicer TP, et al. Small molecule proteostasis regulators that reprogram the ER to reduce extracellular protein aggregation. Elife. 2016; 5 http://dx.doi.org/10.7554/eLife.15550.

Powers ET, Morimoto RI, Dillin A, Kelly JW, Balch WE. Biological and chemical approaches to diseases of proteostasis deficiency. Annu. Rev. Biochem. 2009; 78:959–991. [PubMed: 19298183]

Rappley I, Monteiro C, Novais M, Baranczak A, Solis G, Wiseman RL, Helmke S, Maurer MS, Coelho T, Powers ET, et al. Quantification of transthyretin kinetic stability in human plasma using subunit exchange. Biochemistry. 2014; 53:1993–2006. [PubMed: 24661308]

Razavi H, Palaninathan SK, Powers ET, Wiseman RL, Purkey HE, Mohamedmohaideen NN, Deechongkit S, Chiang KP, Dendle MT, Sacchettini JC, et al. Benzoxazoles as transthyretin amyloid fibril inhibitors: synthesis, evaluation, and mechanism of action. Angew. Chem. Int. Ed. Engl. 2003; 42:2758–2761. [PubMed: 12820260]

Roussel BD, Kruppa AJ, Miranda E, Crowther DC, Lomas DA, Marciniak SJ. Endoplasmic reticulum dysfunction in neurological disease. Lancet Neurol. 2013; 12:105–118. [PubMed: 23237905]

Satpute-Krishnan P, Ajinkya M, Bhat S, Itakura E, Hegde RS, Lippincott-Schwartz J. ER stress-induced clearance of misfolded GPI-anchored proteins via the secretory pathway. Cell. 2014; 158:522–533. [PubMed: 25083867]

Schmidt PM, Sparrow LG, Attwood RM, Xiao X, Adams TE, McKimm-Breschkin JL. Taking down the FLAG! How insect cell expression challenges an established tag-system. PLoS One. 2012; 7:e37779. [PubMed: 22701579]

Schneider F, Hammarstrom P, Kelly JW. Transthyretin slowly exchanges subunits under physiological conditions: a convenient chromatographic method to study subunit exchange in oligomeric proteins. Protein Sci. 2001; 10:1606–1613. [PubMed: 11468357]

Sekijima Y, Wiseman RL, Matteson J, Hammarstrom P, Miller SR, Sawkar AR, Balch WE, Kelly JW. The biological and chemical basis for tissue-selective amyloid disease. Cell. 2005; 121:73–85. [PubMed: 15820680]

Shoulders MD, Ryno LM, Genereux JC, Moresco JJ, Tu PG, Wu C, Yates JR 3rd, Su AI, Kelly JW, Wiseman RL. Stress-independent activation of XBP1s and/or ATF6 reveals three functionally diverse ER proteostasis environments. Cell Rep. 2013; 3:1279–1292. [PubMed: 23583182]

Stangou AJ, Heaton ND, Hawkins PN. Transmission of systemic transthyretin amyloidosis by means of domino liver transplantation. N. Engl. J. Med. 2005; 352:2356. [PubMed: 15930432]

Wyatt AR, Yerbury JJ, Ecroyd H, Wilson MR. Extracellular chaperones and proteostasis. Annu. Rev. Biochem. 2013; 82:295–322. [PubMed: 23350744]

Zhang Q, Kelly JW. Cys10 mixed disulfides make transthyretin more amyloidogenic under mildly acidic conditions. Biochemistry. 2003; 42:8756–8761. [PubMed: 12873136]

Highlights

- Developed assay to measure transthyretin tetramers secreted from mammalian cells
- Highly destabilized TTR tetramers are secreted in non-native conformations
- Pharmacologic chaperoning promotes secretion of destabilized TTR tetramers
- Thapsigargin-induced ER stress reduces the quality of secreted TTR

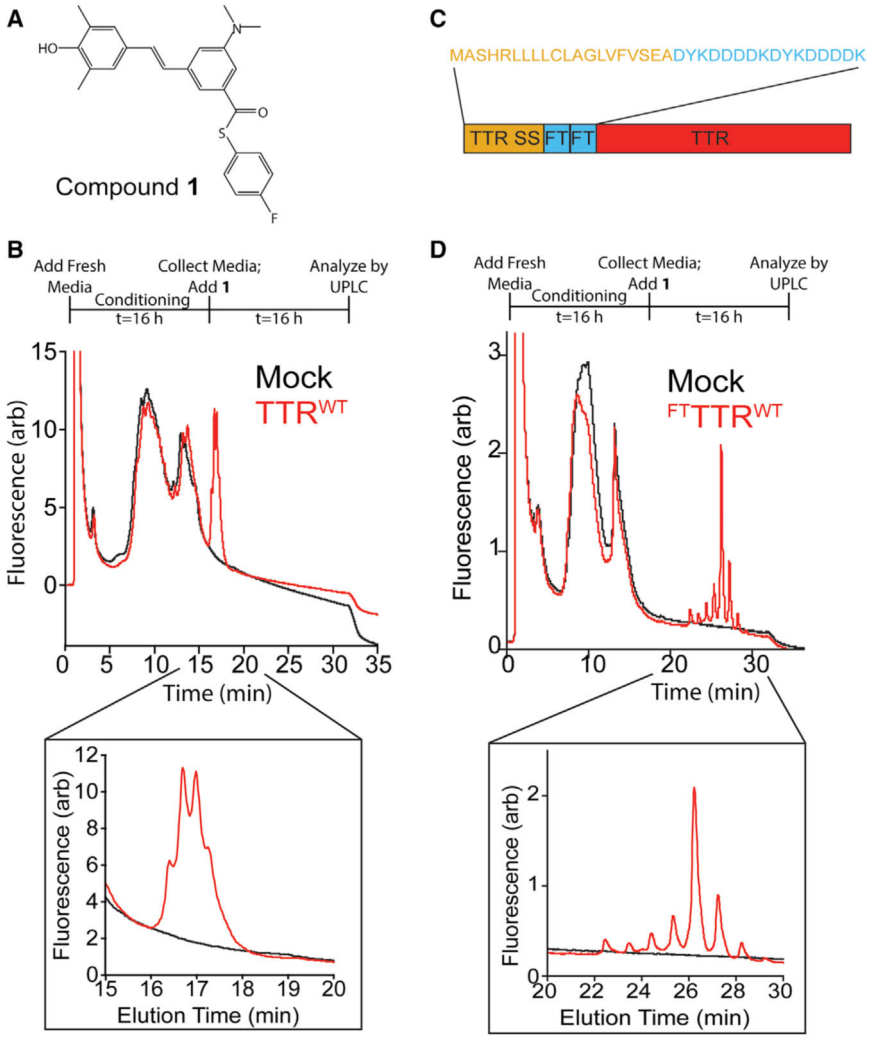

Figure 1. Secreted TTR Tetramers Can Be Detected in Conditioned Media by Compound 1 Conjugate Fluorescence

(A) Structure of the fluorogenic TTR kinetic stabilizer compound **1** (Choi et al., 2010). This molecule covalently reacts with TTR through amide formation to Lys15, liberating the *p*-fluorothiophenol moiety and resulting in compound **1**-TTR conjugate fluorescence.

(B) Plot showing the compound **1**-TTR conjugate fluorescence of media conditioned for 16 hr on mock-transfected HEK293 cells (black) or HEK293 cells expressing TTR^{WT} (red) separated by UPLC anion-exchange chromatography. Compound **1** (10 μM) was incubated with conditioned media for 16 hr prior to analysis. The inset shows compound **1**-TTR conjugate fluorescence for the peaks corresponding to TTR^{WT}. The experimental protocol is described above.

(C) Image showing the ^{FT}TTR sequence containing the TTR ER signal sequence (SS), two FLAG tag sequences, and the TTR coding sequence. The amino acid sequence for the signal sequence and tandem FLAG tag of ^{FT}TTR is shown above.

(D) Plot showing the compound **1**-TTR conjugate fluorescence of media conditioned for 16 hr on mock-transfected HEK293 cells (black) or HEK293 cells expressing $^{FT}TTR^{WT}$ (red) separated by UPLC anion-exchange chromatography. Compound **1** (10 μM) was incubated

with conditioned media for 16 hr prior to analysis. The inset shows compound **1**-TTR conjugate fluorescence for the peaks corresponding to $^{FT}TTR^{WT}$. The experimental protocol is described above.

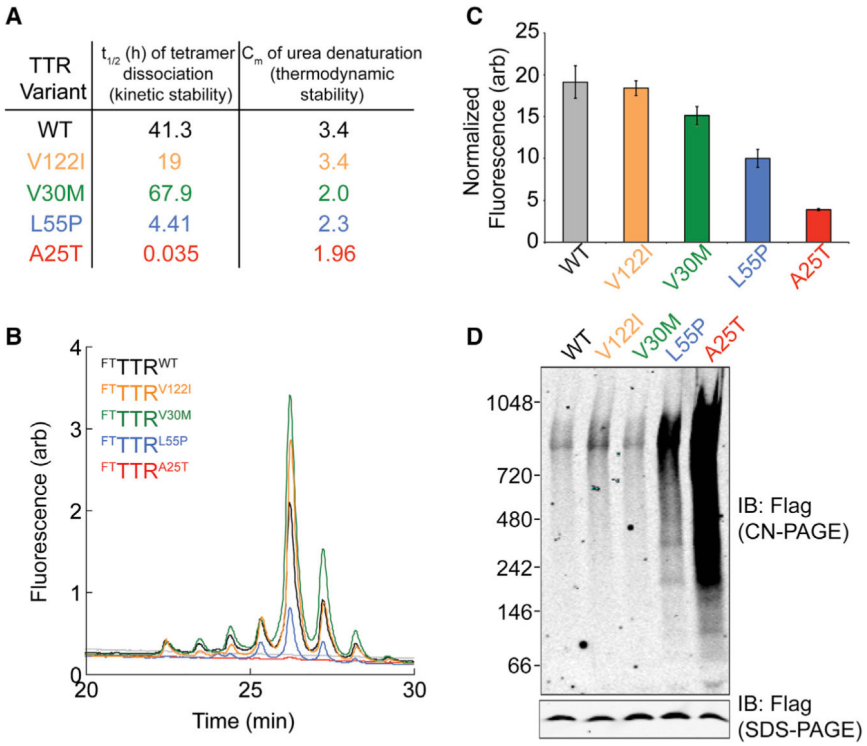

Figure 2. TTR Tetramers Composed of Destabilized Variants Are Unstable in Conditioned Media

(A) Table showing the $t_{1/2}$ of tetramer dissociation (a measure fof kinetic stability) and C_m of urea denaturation (a measure of thermodynamic stability) at 25°C for TTR^{WT} and the disease-associated TTR variants TTR^{V122I}, TTR^{V30M}, TTR^{L55P}, and TTR^{A25T}. These values were reported previously (Sekijima et al., 2005).

(B) Representative plot showing the compound **1**-TTR conjugate fluorescence of media conditioned for 16 hr on HEK293 cells expressing $^{FT}TTR^{WT}$ (black), $^{FT}TTR^{V122I}$ (orange), $^{FT}TTR^{V30M}$ (green), $^{FT}TTR^{L55P}$ (blue), or $^{FT}TTR^{A25T}$ (red). Compound **1** (10 μM) was added to conditioned media for 16 hr prior to analysis by UPLC anion-exchange chromatography.

(C) Graph showing the normalized compound **1**-TTR conjugate fluorescence for plots such as those shown in Figure 2B. Normalization of compound **1**-TTR conjugate fluorescence was performed by integrating the fluorescence signal from all peaks corresponding to the TTR tetramer and then normalizing to the relative amounts of TTR in each conditioned media determined by SDS-PAGE/immunoblotting (see Figure S2B). Error bars show SEM for n = 3.

(D) Clear native (CN)-PAGE and SDS-PAGE immunoblots of media conditioned for 16 hr on HEK293 cells expressing $^{FT}TTR^{WT}$, $^{FT}TTR^{V122I}$, $^{FT}TTR^{V30M}$, $^{FT}TTR^{L55P}$, or $^{FT}TTR^{A25T}$.

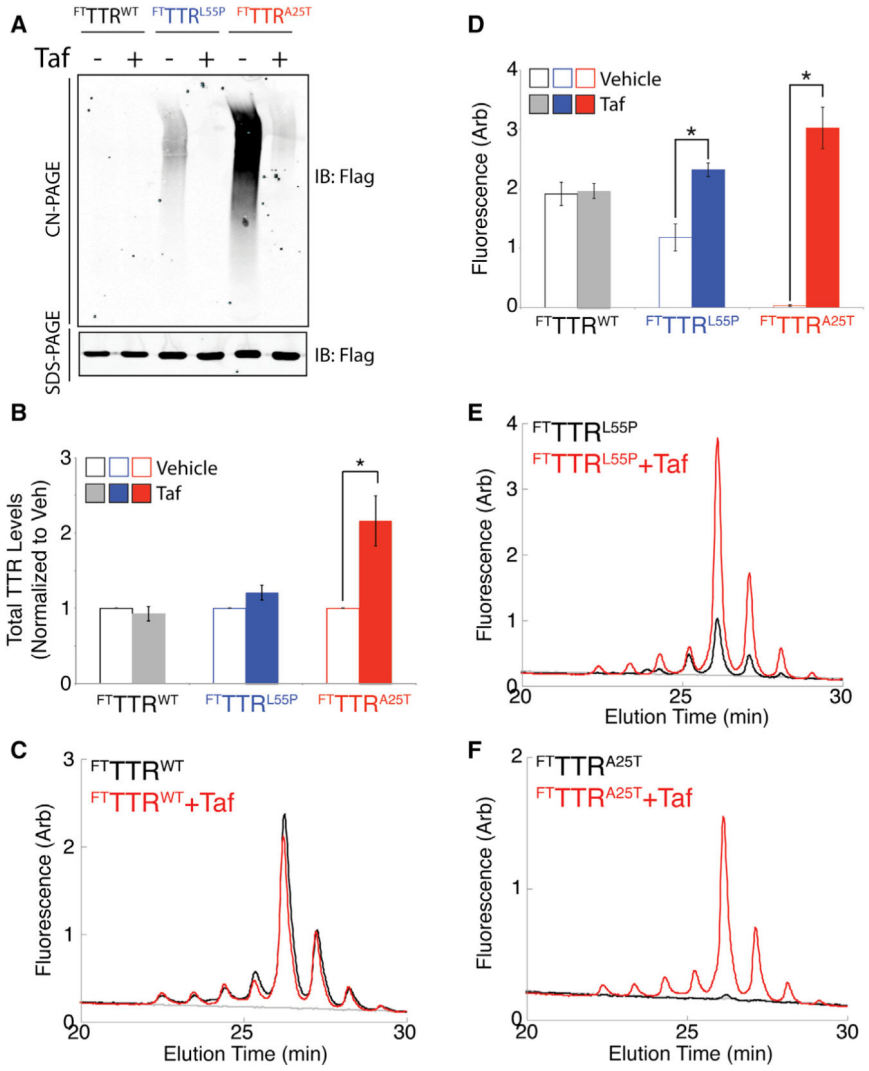

Figure 3. Pharmacologic Chaperoning of TTR Tetramers in the ER Reduces Aggregates and Increases Tetramers of Destabilized TTR Variants in Conditioned Media

(A) Representative CN-PAGE and SDS-PAGE immunoblots of media conditioned for 16 hr on HEK293 cells expressing $^{FT}TTR^{WT}$, $^{FT}TTR^{L55P}$, or $^{FT}TTR^{A25T}$ in the presence or absence of Taf (10 μM).

(B) Graph showing the normalized total amount of $^{FT}TTR^{WT}$ (black), $^{FT}TTR^{L55P}$ (blue), or $^{FT}TTR^{A25T}$ (red) in media conditioned for 16 hr on HEK293 cells expressing these different TTR variants in the presence (solid bars) or absence (open bars) of Taf (10 μM). Total amounts of TTR were measured by SDS-PAGE/immunoblotting as shown in (A). TTR levels were normalized to vehicle-treated cells. Error bars show SEM for n = 3. *$p < 0.05$.

(C) Representative plot showing compound **1**-TTR conjugate fluorescence of media conditioned for 16 hr on HEK293 cells expressing $^{FT}TTR^{WT}$ incubated in the presence (red) or absence (black) of Taf (10 μM). Compound **1** (10 μM) was added to conditioned media for 16 hr prior to analysis by UPLC anion-exchange chromatography.

(D) Graph showing the integrated compound **1**-TTR conjugate fluorescence (including all peaks) for $^{FT}TTR^{WT}$ (gray), $^{FT}TTR^{L55P}$ (blue), and $^{FT}TTR^{A25T}$ (red) in media conditioned

for 16 hr on HEK293 cells expressing the indicated ^{FT}TTR variant in the presence (solid bars) or absence (open bars) of Taf (10 μM). Representative plots are shown in (C), (E), and (F). Error bars show SEM for n = 3. *p < 0.05.

(E) Representative plot showing compound **1**-TTR conjugate fluorescence of media conditioned for 16 hr on HEK293 cells expressing ^{FT}TTR^{L55P} incubated in the presence (red) or absence (black) of Taf (10 μM). Compound **1** (10 μM) was added to conditioned media for 16 hr prior to analysis by UPLC anion-exchange chromatography.

(F) Representative plot showing compound **1**-TTR conjugate fluorescence of media conditioned for 16 hr on HEK293 cells expressing ^{FT}TTR^{A25T} incubated in the presence (red) or absence (black) of Taf (10 μM). Compound **1** (10 μM) was added to conditioned media for 16 hr prior to analysis by UPLC anion-exchange chromatography.

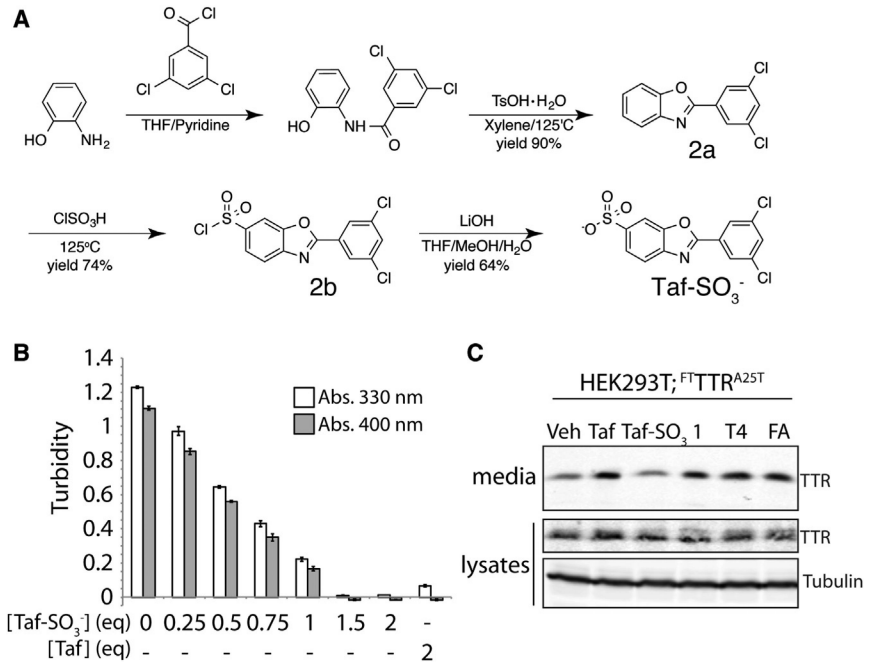

Figure 4. Tafamidis-Sulfonate (Taf-SO_3^-) Is a Non-Cell-Permeable Kinetic Stabilizer of the TTR Tetramer

(A) Synthetic scheme used to prepare Taf-SO_3^-.

(B) Graph showing the acid-induced aggregation of TTR^{WT} (3.6 μM tetramer) at pH 4.4 measured by turbidity at 400 nm (gray) or 330 nm (white). Taf or Taf-SO_3^- was added at the indicated molar equivalents to the TTR tetramer (3.6 μM). Error bars show SEM for n = 3.

(C) Immunoblot showing TTR in media conditioned on HEK293 cells expressing $^{FT}TTR^{A25T}$ in the presence of TTR tetramer kinetic stabilizers Taf, Taf-SO_3^-, **1**, thyroxine (T4), or flufenamic acid (FA) (10 μM). The lysate samples are shown as a control.

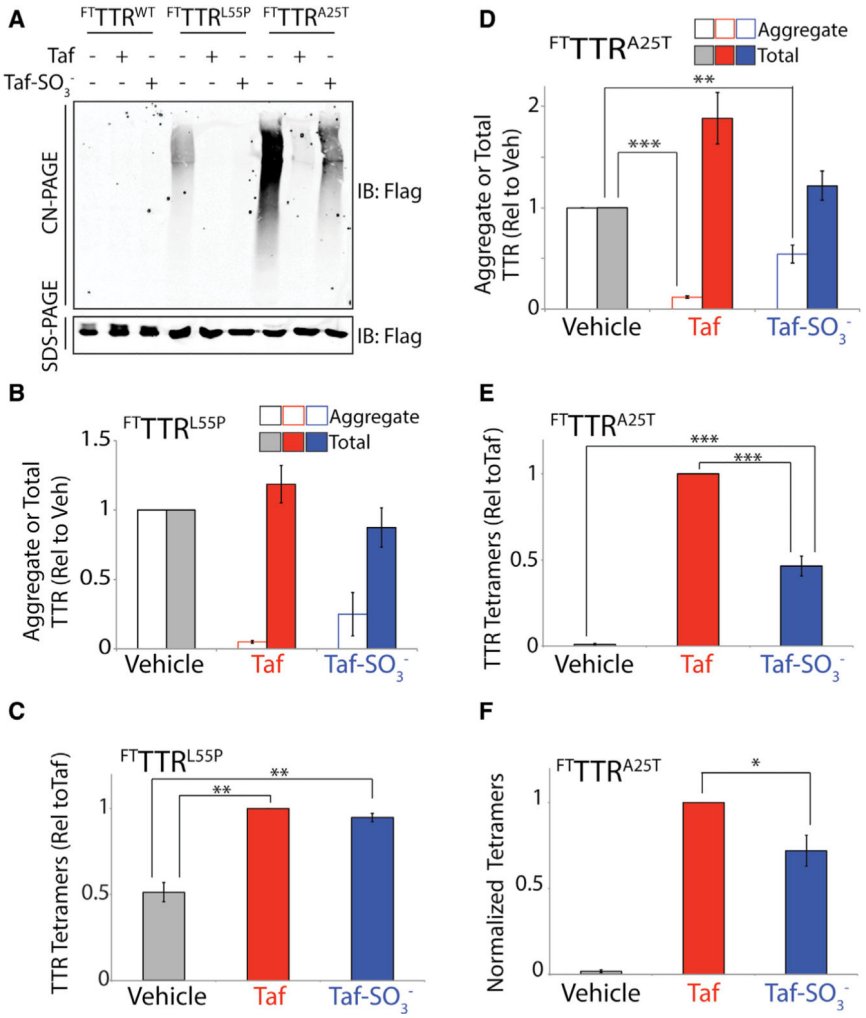

Figure 5. Highly Destabilized TTR Variants Can Be Secreted as Native Tetramers and in Non-Tetrameric Conformations

(A) Representative CN-PAGE and SDS-PAGE immunoblots of media conditioned for 16 hr on HEK293 cells expressing $^{FT}TTR^{WT}$, $^{FT}TTR^{L55P}$, or $^{FT}TTR^{A25T}$ in the presence of Taf (10 μM) or Taf-SO_3^- (all at 10 μM).

(B) Graph showing the quantification of aggregate (open bars; measured by CN-PAGE) or total (solid bars; measured by SDS-PAGE) $^{FT}TTR^{L55P}$ in media conditioned on HEK293 cells in the presence of vehicle (gray), Taf (10 μM; red), or Taf-SO_3^- (10 μM; blue). Representative immunoblots are shown in (A). Error bars show SEM for n = 3.

(C) Graph showing tetramer levels in media conditioned on HEK293 cells expressing $^{FT}TTR^{L55P}$ in the presence of vehicle (gray), Taf (10 μM; red), or Taf-SO_3^- (10 μM; blue). Tetramer levels were quantified by integrating compound **1**-TTR conjugate fluorescence measured by UPLC and are shown relative to Taf-treated cells. A representative UPLC trace is shown in Figure S4A. Error bars show SEM for n = 4. **p < 0.01.

(D) Graph showing the quantification of aggregate (open bars; measured by CN-PAGE) or total (solid bars; measured by SDS-PAGE) $^{FT}TTR^{A25T}$ in media conditioned for 16 hr on HEK293 cells in the presence of vehicle (gray), Taf (10 μM; red), or Taf-SO_3^- (10 μM;

blue). Representative immunoblots are shown in (A). Error bars show SEM for n = 8. ***p < 0.005, **p < 0.01.

(E) Graph showing tetramer levels in media conditioned for 16 hr on HEK293 cells expressing $^{FT}TTR^{A25T}$ in the presence of vehicle (gray), Taf (10 μM; red), or Taf-SO_3^- (10 μM; blue). Tetramer levels were quantified by integrating compound **1**-TTR conjugate fluorescence measured by UPLC and are shown relative to Taf-treated cells. A representative UPLC trace is shown in Figure S4B. Error bars show SEM for n = 4. ***p < 0.005.

(F) Graph showing the normalized compound **1**-TTR conjugate fluorescence of TTR tetramers in media conditioned for 16 hr on HEK293 cells expressing $^{FT}TTR^{A25T}$ in the presence of vehicle (gray), Taf (10 μM; red), or Taf-SO_3^- (10 μM; blue). Compound **1**-TTR conjugate fluorescence was normalized to the average relative amounts of total $^{FT}TTR^{A25T}$ (measured by SDS-PAGE; A) to account for differences in total protein in media prepared in the presence of Taf or Taf-SO_3^-. Error bars show SEM for n = 4. *p < 0.05.

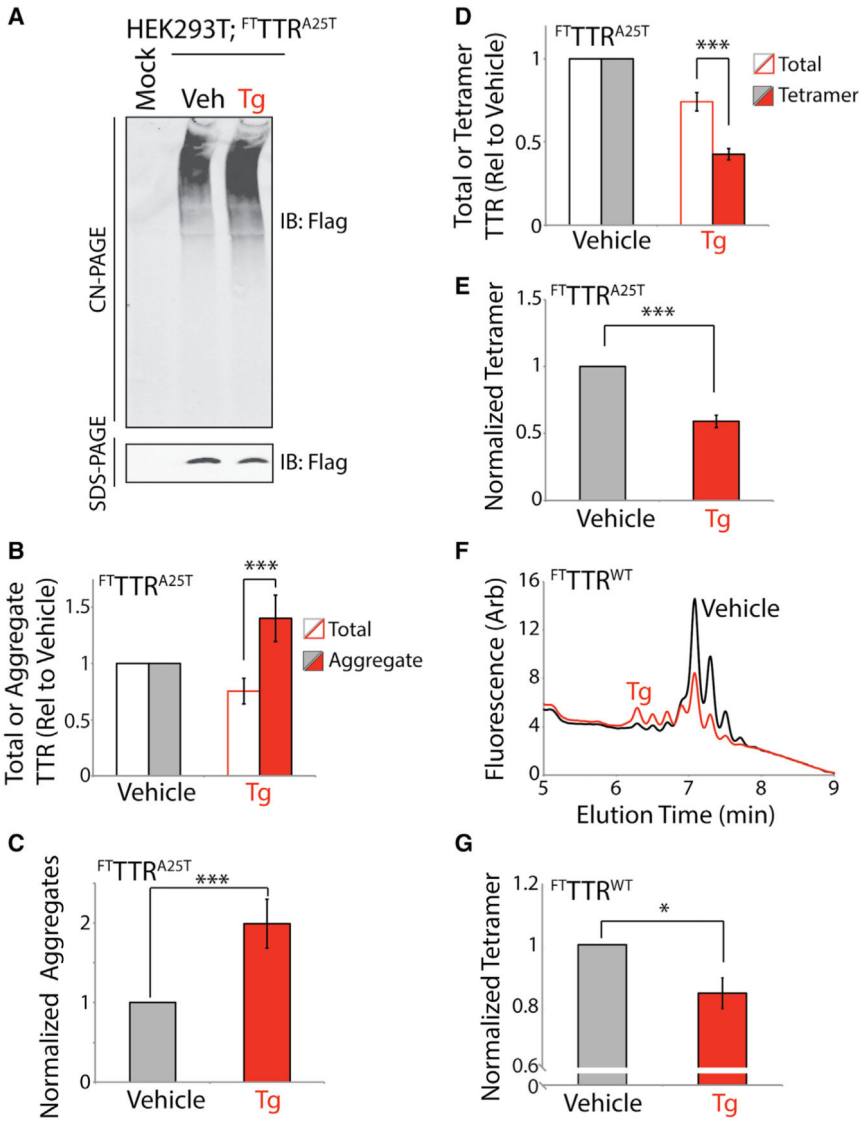

Figure 6. Thapsigargin-Induced ER Stress Reduces Secretion of $^{FT}TTR^{A25T}$ as Tetramers and Increases Extracellular TTR Aggregates

(A) Representative CN-PAGE and SDS-PAGE immunoblots of media conditioned for 16 hr on HEK293 cells expressing $^{FT}TTR^{A25T}$ in the presence of vehicle or thapsigargin (Tg) (0.5 μM). All media were conditioned in the presence of Taf-SO_3^- (10 μM).

(B) Graph showing total TTR (open bars; measured by SDS-PAGE) and aggregate TTR (closed bars; measured by CN-PAGE) in media conditioned for 16 hr on HEK293 cells expressing $^{FT}TTR^{A25T}$ in the presence of vehicle (gray) or Tg (red; 0.5 μM). All media were conditioned in the presence of Taf-SO_3^- (10 μM). Representative immunoblots are shown in (A). Data are shown relative to vehicle-treated cells. Error bars show SEM for n = 12. ***p < 0.005.

(C) Graph showing normalized TTR aggregates in the conditioned media described in (A) and (B). Normalized aggregates were calculated by dividing the relative amounts of aggregate by the total amount of TTR in each sample measured by SDS-PAGE. This

normalization is necessary to account for the reduced total $^{FT}TTR^{A25T}$ levels observed in Tg-treated cells. Error bars show SEM for n = 12. ***p < 0.005.

(D) Graph showing total TTR (open bars; measured by SDS-PAGE) and tetrameric TTR (closed bars; measured by integrated compound **1**-TTR conjugate fluorescence from UPLC traces) in media conditioned for 16 hr on HEK293 cells expressing $^{FT}TTR^{A25T}$ in the presence of vehicle (gray) or Tg (red; 0.5 μM). All media were conditioned in the presence of Taf-SO_3^- (10 μM). A representative UPLC trace is shown in Figure S5B. Data are shown relative to vehicle-treated cells. Error bars show SEM for n = 15. ***p < 0.005.

(E) Graph showing normalized TTR tetramers in the conditioned media described in (D). Normalized tetramers were calculated by dividing the relative tetramer levels by the total amount of TTR in each sample measured by SDS-PAGE. This normalization is necessary to account for the reduced total $^{FT}TTR^{A25T}$ levels observed in Tg-treated cells. Error bars show SEM for n = 15. ***p < 0.005.

(F) Representative plot showing compound **1**-TTR conjugate fluorescence of media conditioned for 16 hr on HEK293 cells expressing $^{FT}TTR^{WT}$ in the presence (red) or absence (black) of Tg (0.5 μM). Media were conditioned in the presence of Taf-SO_3^- (10 μM). Compound **1** (10 μM) was added to conditioned media for 16 hr prior to analysis by UPLC anion-exchange chromatography.

(G) Graph showing normalized $^{FT}TTR^{WT}$ tetramers in the conditioned media described in (F). Normalized tetramers were calculated by dividing the relative tetramer levels by the total amount of TTR in each sample measured by SDS-PAGE. This normalization is necessary to account for the reduced total $^{FT}TTR^{WT}$ levels observed in Tg-treated cells. Independent quantifications of total $^{FT}TTR^{WT}$ (measured by SDS-PAGE) and tetrameric $^{FT}TTR^{WT}$ (measured by integrated compound **1**-TTR conjugate fluorescence from UPLC traces) in these conditioned media are shown in Figure S5G. Error bars show SEM for n = 6. *p < 0.05.